Lawrence Berkeley National Laboratory
Recent Work

Title
Effects of Presipitate Distribution on 293 K and 77 K Properties of 2090-T81 Weldments

Permalink
https://escholarship.org/uc/item/8xn1m1p2

Authors
Sunwoo, A.J.
Miyasato, S.
Morris, J.W.

Publication Date
1989-06-01

eScholarship.org Powered by the California Digital Library
University of California

LBL-27380

Center for Advanced Materials

CAM

Presented at the CEC/ICMC, Los Angeles, CA,
July 24–28, 1989, and to be published in the Proceedings

Effects of Precipitate Distribution on 293 K and 77 K Properties of 2090-T81 Weldments

A.J. Sunwoo, S. Miyasato, and J.W. Morris, Jr.

June 1989

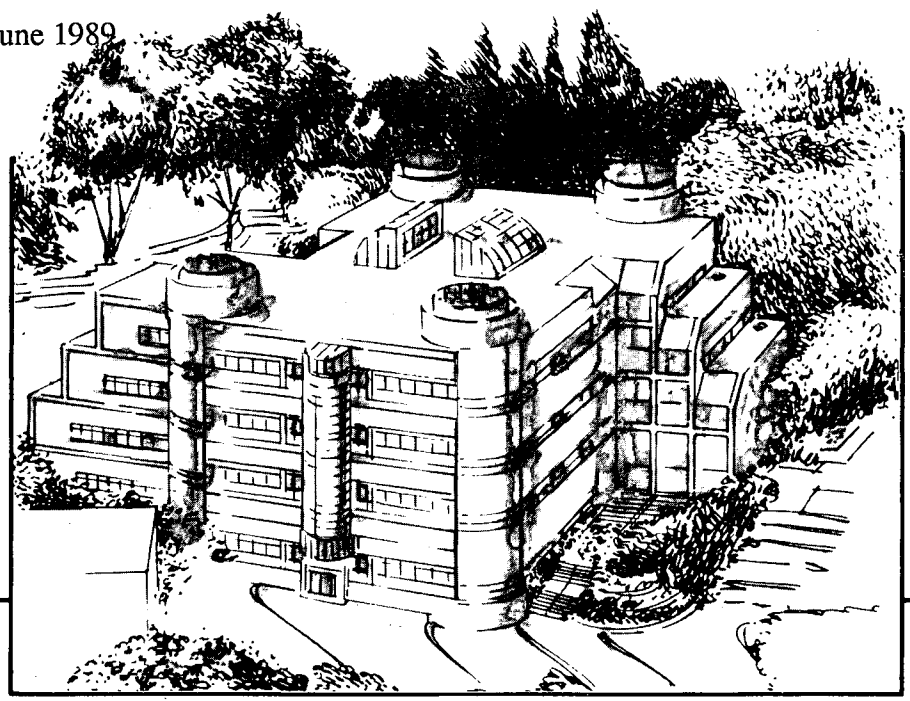

Materials and Chemical Sciences Division

Lawrence Berkeley Laboratory • University of California

ONE CYCLOTRON ROAD, BERKELEY, CA 94720 • (415) 486-4755

Prepared for the U.S. Department of Energy under Contract DE-AC03-76SF00098

LOAN COPY
Circulates
for 2 weeks
Copy 2
Bldg. 50 Library.
LBL-27380

DISCLAIMER

This document was prepared as an account of work sponsored by the United States Government. While this document is believed to contain correct information, neither the United States Government nor any agency thereof, nor the Regents of the University of California, nor any of their employees, makes any warranty, express or implied, or assumes any legal responsibility for the accuracy, completeness, or usefulness of any information, apparatus, product, or process disclosed, or represents that its use would not infringe privately owned rights. Reference herein to any specific commercial product, process, or service by its trade name, trademark, manufacturer, or otherwise, does not necessarily constitute or imply its endorsement, recommendation, or favoring by the United States Government or any agency thereof, or the Regents of the University of California. The views and opinions of authors expressed herein do not necessarily state or reflect those of the United States Government or any agency thereof or the Regents of the University of California.

LBL 27380

EFFECTS OF PRECIPITATE DISTRIBUTION ON 293 K AND 77 K PROPERTIES OF 2090-T81 WELDMENTS

A. J. Sunwoo, S. Miyasato and J. W. Morris, Jr.

Center for Advanced Materials
Materials and Chemical Sciences Division
Lawrence Berkeley Laboratory
1 Cyclotron Road
Berkeley, CA 94720

and

Department of Materials Science and Mineral Engineering
University of California

June 1989

This work was jointly supported by the ALCOA Laboratories and by the Director, Office of Energy Research, Office of Basic Energy Science, Materials Science Division of the U. S. Department of Energy under Contract No. *DE-AC03-76SF00098*

EFFECTS OF PRECIPITATE DISTRIBUTION ON 293 K AND 77 K PROPERTIES OF 2090-T81 WELDMENTS

A. J. Sunwoo, S. Miyasato, and J. W. Morris, Jr.

Center for Advanced Materials, Lawrence Berkeley Laboratory, and
Department of Materials Science and Engineering, University of California, Berkeley

Although 2090-T81 precipitation behavior has been well documented, the weld precipitation behavior has not been as-well characterized. The purpose of this study is to characterize the EB and GTA fusion zone precipitates and their distribution and to correlate the microstructure to 293 K and 77 K properties. The base metal strengths are greatly enhanced by a homogeneous distribution of T_1 precipitates at 293 K and 77 K, but the presence of T_1 and T_2 at the boundaries has an adverse effect on the elongation at 77 K. The weld strengths are limited by a lack of strengthening precipitates. Fusion zone embrittlement is caused by the formation of Cu-Fe containing film and strain localization at the dendrite boundaries.

INTRODUCTION

2090-T81 alloy has very good mechanical properties at room and cryogenic temperatures, but good weldability is also an essential prerequisite for some applications [1,2]. Much recent attention has been devoted to weldability studies and limited attention given to welding metallurgy and the understanding of the mechanisms, which control the properties. Ideally, compatibility in strength, toughness, and ductility is desired between the base metal and the weld; however, without proper thermal-mechanical processing the weld properties are always inferior to the base metal properties [3-5].

Contrary to earlier work by Martukanitz et al. [6], 2090 is very weldable and has acceptable engineering properties [7,8]. However, there is a strong inverse relationship between the weld strength and elongation with post-weld aging [9]. As the strength increases, the elongation decreases rapidly even at early stages of aging. Although this inverse relationship has been attributed to a solute gradient transforming to a precipitate gradient thereby causing strain localization at the boundary, there is limited literature available dealing with the characterization of the fusion zone microstructure. The purpose of this study is to characterize the fusion zone precipitates and their distribution and to correlate the microstructure to the 293 K and 77 K properties of peak-aged 2090 weldments. In order to simplify an already complicated system and to have better control over the properties, only the welding processes are varied with overall composition held constant. Thus, the differences in the properties will be governed only by the precipitates and their distribution.

EXPERIMENTAL PROCEDURE

The nominal chemical composition of 2090 is, in wt-%, 3.0Cu-2.2Li-0.12Zr-Al. The as-received 2090 sheet was in T3 temper (solution heat treated and stretched 4.6%). The weld coupons were cut to usable dimensions, and the surfaces were machined to remove the

processing oxide and to eliminate distortion. Prior to welding, the weld coupons were chemically cleaned with 5 vol-% sodium hydroxide in water followed by nitric acid.

Electron beam (EB) and gas tungsten arc (GTA) welding were utilized and the heat inputs needed to produce a full penetration weld were 45 J/mm and 310 J/mm, respectively. GTA welding was conducted on a water-cooled chill block in an argon atmosphere and EB welding in vacuum (10^{-4} torr). Autogenous, bead-on-plate welds were produced transverse to the longitudinal direction of the T3 tempered base metal for both processes.

After the weld reinforcements were machined off, the final thickness of the weldments was reduced from 3.2mm to 2.54mm. The base metal and weldments were post-weld aged at 160°C for 32 hours to obtain peak-aged condition. A 25.4mm composite gage length consisting of both fusion zone and base metal was used for the welded tensile specimens, and the base metal specimens were made in longitudinal direction. The tension tests were conducted at 293 K and at 77 K.

Transmission electron microscopy (TEM) specimens were made from the base metal, and EB and GTA fusion zones. The specimens were prepared by polishing the disks to 0.125mm thickness and jet-polished using 25 vol-% nitric acid in methanol at -30°C. To minimize preferential attack of intermetallics in the welded specimens, a high intensity fiber optic light source and a constant voltage of 20V were used. The foils were viewed at 100kV using a Philips EM 301. Energy dispersive x-ray (EDX) analysis was performed using scanning transmission electron microscope attached on a Philips EM 400.

RESULTS

Tensile Properties

The tensile properties of the base metal, EB and GTA weldments are presented in Table 1. In the peak-aged condition, the base metal strengths were high with relatively good elongation at 293 K. Although the 77 K strengths were higher by at least 10%, the elongation decreased by 45%. The specimens failed prematurely in shear at the clips, caused by notch sensitivity of 2090.

Table 1. Peak-aged tensile properties of base metal, EB and GTA weldments at 293 K and at 77 K.

	σ_{YS} MPa	σ_{UTS}[a] MPa	Total Elongation (%)
293 K			
Base Metal:	574	608	9.4
EBW:	438	445[a]	0.3
GTAW:	314	372[a]	0.8
77 K			
Base Metal:	634	712[a]	5.2
EBW:	476	493[a]	0.3
GTAW	320	375[a]	0.6

[a] Fracture strength.

Even in the peak-aged condition, the strength mismatch between the base metal and the welds was persistent. EB weldments showed an increase in strengths similar to the base metal with decreasing temperatures but the strength mismatch was maintained, with a joint efficiency of about 75%. (Joint efficiency is a ratio of weldment yield strength to base metal yield strength.) The EB weldment elongation was very low, 0.3%.

GTA weldments, on the other hand, had both low strength and low elongation. A negligible increase in strengths was found at 77 K, and the joint efficiency decreased from 55% to 50%. At both temperatures, EB and GTA weldments failed prematurely in the fusion zone with little observable deformation.

Fractography

Figure 1 shows the SEM fractographs of the base metal, and EB and GTA weldments tested at 77 K: the fracture appearance for each condition is unique and remains unchanged for both 273 K and 77 K. The fracture mode for the base metal is, as commonly seen, mixed ductile-transgranular fracture with delamination in the through thickness direction, Fig. 1a. EB weldments with equiaxed dendrite morphology showed a predominantly interdendritic failure, Fig. 1b.

GTA weldments failed in a mixed fracture mode, ductile dimples with secondary cracks along the dendrite boundaries, Fig. 1c. The dendrites appeared to have necked and the failure occurred as the voids coalesced. Because of the nature of cellular dendrite morphology (high aspect ratio, with the long axis in tensile direction) the individual dendrites may act as independent tensile specimens during deformation; and because 2090 has overall low strain hardening rate, strain localization may cause premature failure. This simple view of the fusion zone deformation becomes complicated with the aging. TEM was utilized to develop a understanding of the precipitation behavior and its influence on the properties.

Transmission Electron Microscopy

The mechanical properties of precipitate-strengthened 2090-T81 depend upon the size, distribution, and volume fraction of the precipitates. The strengthening phases are $\delta'(Al_3Li)$, $\theta'(Al_2Cu)$, and $T_1(Al_2CuLi)$ where both θ' and T_1 have plate morphology and T_1 is the primary strengthening phase. Moreover, T_1, an equilibrium phase along with $T_2(Al_6CuLi_3)$, is shown to form heterogeneously at the boundaries [10,11].

Figures 2a through c are a series of centered dark field (CDF) images from the same area of base metal taken using [110] zone axis: Fig. 2a is imaged in the 001 δ' CDF; Figs. 2b and 2c are two edge-on variants of T_1 CDF. The δ' CDF micrograph showed a distinct δ'- and θ'-precipitate free zone (PFZ) adjacent to the high-angle boundary with T_2 precipitates outlining the boundary (arrowed in Fig.2). The PFZ was not as obvious at the low-angle boundary even though T_1 precipitates were present at the boundary. The PFZ developed as a consequence of having both equilibrium phases concurrently present up to and at the high-angle boundary, where the precipitates competed for solute. However, the effects of PFZ on the properties should be a minimal since T_1 precipitates form uniformly up to the boundaries. However, the presence of T_1 and T_2 phases at the boundaries should have an effect on the elongation.

As a result of the solute segregation in the fusion zone, precipitation occurred mostly at the vicinity of the boundaries. Thus, PFZ was not found in EB nor GTA welds. Instead, the EB fusion zone consisted of localized distributions of θ' and T_1 with comparatively homogeneous distribution of δ' within the dendrite, Fig. 3. In contrast, the GTA fusion zone

consisted of high concentrations of mostly δ' and θ' precipitates up to the boundary with sparsely distributed T_1 within the matrix, Fig. 4.

The EB and GTA fusion zone boundaries were decorated with intermetallic constituents and a continuous film. Figure 5 shows two edge-on variants of T_1 CDF images of the EB dendrite taken using [110] zone axis; Fig. 5a shows T_1 precipitates on the boundary and Fig. 5b continuous film/intermetallic formation on the boundary. These intermetallics and film were present in all the welded specimens but not in the base metal specimens.

The EDX analysis was performed throughout the EB fusion zone to locate Cu, since there were limited T_1 and θ' precipitates present within the dendrites and also to determine the composition of the intermetallics. The analysis indicated that the average composition of the EB fusion zone was similar to the base metal, but, locally, inhomogeneities in Cu distribution were found with positive Cu gradients to the boundaries. In addition, there was also a variation in the intermetallics compositions at the boundary: the analysis of the dendrite boundary shown in Fig. 5b detected Cu and some Fe while some boundary constituents were composed of very high concentrations of Cu, Si, and Fe. The base metal analysis on the other hand consisted of expected composition of 2090 but no detectable segregation of Fe or Si was found.

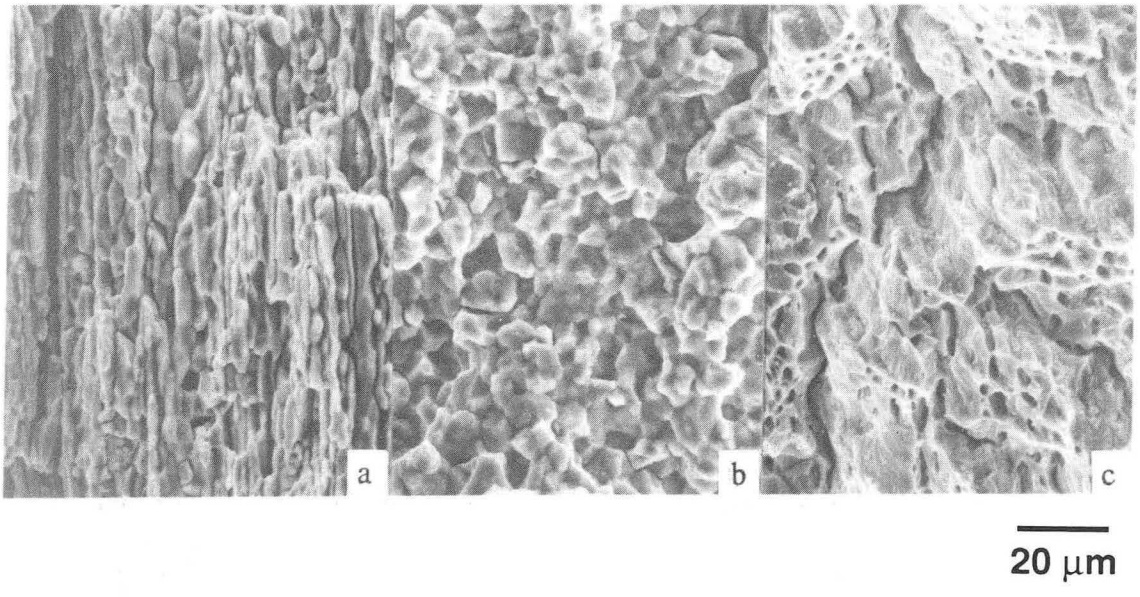

Fig. 1. SEM fractographs of: (a) base metal; (b) EB weldment; and (c) GTA weldment tested at 77 K. (XBB897-5597-B)

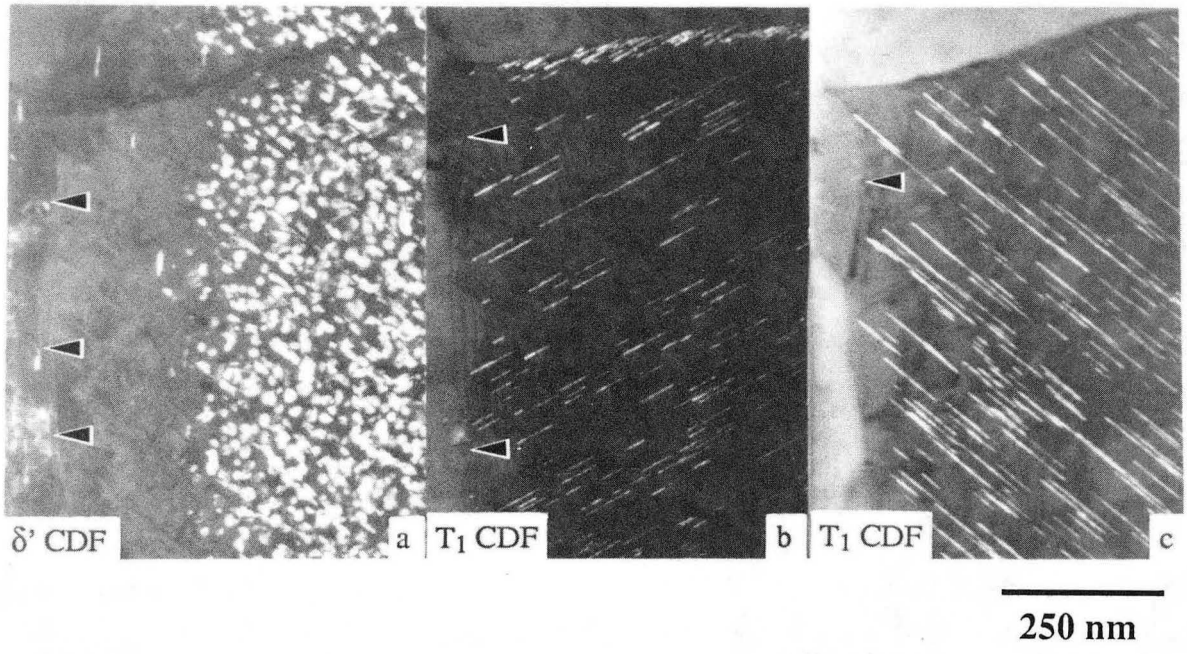

Fig. 2. TEM micrographs from the same area of peak-aged base metal taken using [110] zone axis: (a) 001 δ' CDF; (b) two edge-on variants of T_1 CDF. (XBB897-5598-A)

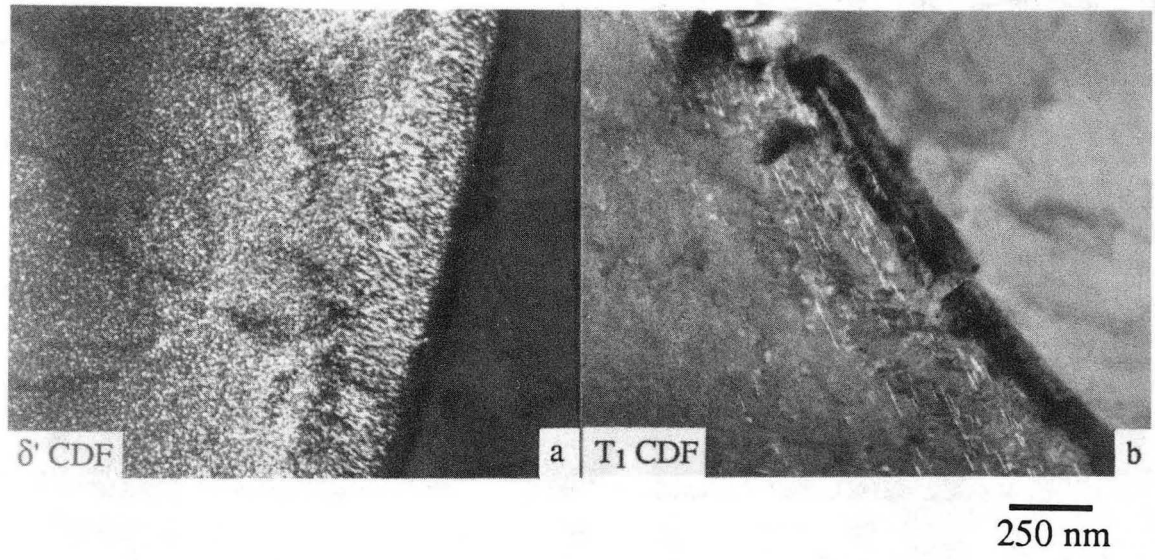

Fig. 3. TEM micrographs of peak-aged EB fusion zone taken using [110] zone axis: (a) 001 δ' CDF; and (b) edge-on variant of T_1 CDF. (XBB897-5880-A)

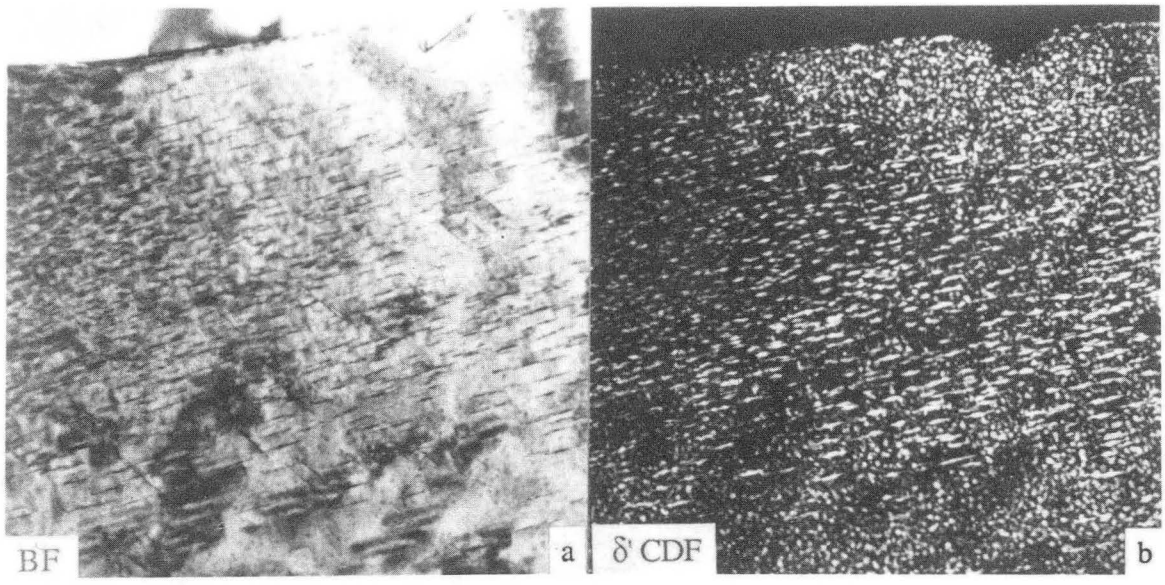

Fig. 4. TEM micrographs of GTA fusion zone taken using [110] zone axis: (a) bright field; and (b) 001 δ' CDF. (XBB897-5784-A)

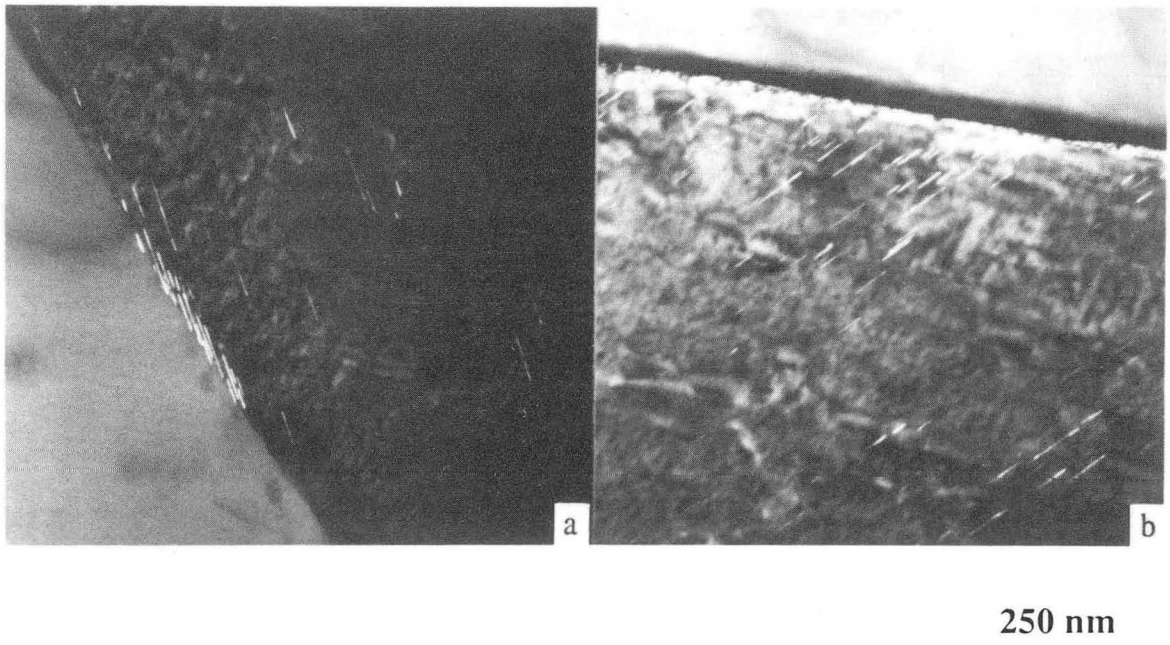

Fig. 5. TEM micrographs of peak-aged EB fusion zone taken using [110] zone axis: (a) and (b) two edge-on variants of T_1 CDF. (XBB897-5783-A)

DISCUSSION

2090-T81 obtains its good mechanical properties through a homogeneous distribution of strengthening precipitates. TMP prior to aging not only led to a homogeneous distribution of T_1 phase within the matrix, but also T_1 formation at the subgrain boundaries. As a dislocation moves through the matrix, the motion is impeded by the T_1 precipitates, yielding higher strengths. At lower temperatures, there is less thermal activation leading to a greater resistance to dislocation motion and causing an increase in strain hardening rate and in strength [12] However, the presence of equilibrium precipitates at the boundaries has an adverse effect on the elongation. At the boundary precipitates the microvoid formation occurs due the stress and strain imcompatibility between the incoherent and hard precipitates and the adjacent matrix and as these voids coalesce, subsequently results in failure [13]. At lower temperatures, this incompatibility will be greater and failure tends to occur prematurely at the boundary. Thus, a significant decrease in the elongation has been observed at 77 K.

The strength difference between the base metal and the welds is caused by the lack of strengthening T_1 precipitates in the bulk of the fusion zone and its localization around the boundaries. Segregation of Cu to the boundaries limits the amount of Cu available to precipitate T_1 phase. Although Cu segregation is prominent at the EB boundaries, an EDX line scan across the GTA boundaries indicates an even greater degree of Cu segregation than that of EB boundaries [9]. With a greater Cu segregation to the boundaries, there is less Cu available to precipitate T_1 phase in the GTA matrix. Hence the dissimilarity in weld strengths must also be attributed to the difference in the number of T_1 precipitates present in the matrix since T_1 precipitate formation is dependent on Cu content. Inhomogeneities in T_1 distribution are observed.

Fusion zone embrittlement is observed in the aged condition and is a result of the Cu-Fe containing film formation at the dendrite boundaries, which causes low boundary strength, and strain localization induced by precipitates near the boundaries. However, in the as-welded and solution heat treated (SHT) conditions EB and GTA weldment elongations are about 4% and greater than 15%, respectively. Moreover, in the solution heat treated condition the EB weldment has failed in the base metal.

This continuous film formation is not a problem for the base metal since Fe or Si is distributed more homogeneously. However during welding, resolidification occurs and the solutes are rejected to the boundaries and create the solute enriched region at the boundaries. Even if the local Fe and Si contents in the base metal are negligible, detrimental effect on the elongation is incurred when they accumulate at the boundaries.

An improvement in the elongation is feasible with the filler metal additions even though the strength mismatch between the base metal and the weld persists, [14]. As yet, there is no effective method of increasing the strength of the weld without the post-weld aging. In order to minimize the strength mismatch and improve the weldment elongation, further study in the aging treatment for the fusion zone is essential.

CONCLUSIONS

The purpose of this study is to characterize the fusion zone precipitates and their distribution and to correlate the microstructure to the properties. When the precipitate distribution of the base metal is compared to those of the EB and GTA fusion zones, the effect of thermal mechanical processing of the base metal is obvious. With a homogeneous distribution of T_1 precipitates, the base metal strengths are greatly enhanced at 293 K and at

77 K, but the presence of T_1 and T_2 at the boundaries has an adverse effect on the elongation at 77 K.

The EB and GTA fusion zone strengths are limited by a lack of strengthening precipitates available in the matrix due to a severe Cu segregation to the boundaries. Fusion zone embrittlement is caused by the formation of Cu-Fe containing film and strain localization at the boundaries. The joint efficiencies of EB and GTA weldments are 75% and 55% at 293 K and 75% and 50% at 77 K, respectively, with unfavorably low weldment elongations.

ACKNOWLEDGEMENT

Authors would like to thank the Aluminum Company of America for providing the materials, and B. L. Olsen and D. E. Hoffman of Lawrence Livermore National Laboratory for producing the electron beam welds. This research is funded by the Director, Office of Energy Research, Office of Basic Energy Science, Material Sciences Division of the U.S. Department of Energy under Contract No. DE-AC03-76SF00098.

REFERENCES

1. J. Glazer, S.L. Verzasconi, E.N.C. Dalder, W. Yu, R.A. Emigh, R.O. Ritichie, and J.W. Morris, Jr., Adv. Cryo. Eng., 32:397 (1986).
2. J.W. Morris, and J. Glazer, Cryo. Mat. 1988, Proc. from Int'l Cryo. Conf. Proc., Shenyang, China, 2:713 (1988).
3. F.G. Nelson, J.G. Kaufman, and E.T. Wanderer, Adv.Cryo Eng., 14:71 (1969).
4. M.J. Strum, L.T. Summers, and J.W. Morris, Jr., Welding Journal, 9:235 (1983).
5. J.W. Chan, Cryogenic Mechanical Properties of 18Mn-5Ni-0.2N weldments, M.S. Thesis, University of California, Berkeley (1987).
6. R.P. Martukanitiz, C.A. Natalie, and J.O. Knoefel, Alcoa PREN Division Report 52-87-20 (1987).
7. J.R. Kerr and R.E. Merino, Al-Li-V, to be published in Conf. Proc. (1989).
8. C.C. Griffee, G.A. Jensen, and T.L. Reinhart, same as Ref. 7.
9. A.J. Sunwo and J.W. Morris, Jr., Welding Journal, 68:262S (1989).
10. M.H. Tosten, A.K. Vasudevan, and P.R. Howell, Met. Trans. A, 19A:51 (1988).
11 A.J. Shaksheff, D.S. McKarmaid, and P.J. Gregson, Materials Letters, 7:353 (1989).
12. J. Glazer, S.L. Verzasconi, R.R Sawtell, and J.W. Morris, Jr., Metall. Trans., 18A:1695 (1987).
13. A.K. Vasudevan and R.D. Doherty, Acta Metall. 35:1193 (1987).
14. A.J. Sunwoo and J.W. Morris, Jr., same as Ref. 7.

LAWRENCE BERKELEY LABORATORY
CENTER FOR ADVANCED MATERIALS
1 CYCLOTRON ROAD
BERKELEY, CALIFORNIA 94720